Electromagnetic dissociation of relativistic heavy ions

W. J. Llope and P. Braun-Munzinger
Department of Physics, State University of New York at Stony Brook, Stony Brook, New York 11794
(Received 12 January 1990)

A framework is developed for the quantitative analysis of the electromagnetic dissociation of relativistic nuclei. This includes treatment of multiple excitations of the giant dipole resonance, coupled with calculations of the fragmentation probabilities in the framework of the statistical model. Experimental data on electromagnetic projectile dissociation at relativistic energies are compared to the model predictions and shown to be consistent with first-order excitation followed by statistical decay of the excited nucleus. Strategies for the search for multiple excitation processes and subsequent rare decay modes are discussed.

I. INTRODUCTION

In the last decade, beams of atomic nuclei at relativistic energies have become available from accelerators such as the Bevalac at the Lawrence Berkeley Laboratory, the Alternating Gradient Synchrotron (AGS) at Brookhaven, and the Super Proton Synchrotron (SPS) at CERN. In collisions between two such nuclei their relativistically contracted electromagnetic fields can lead to extremely large probabilities for electromagnetic excitations. In fact, for the heaviest nuclei at ultrarelativistic energies, the cross section for excitation above the particle threshold can be on the order of *hundreds of barns*, by far exceeding the geometric cross section. In a typical distant collision, i.e., with an impact parameter larger than R_T+R_P, the radii of target and projectile, respectively, this electromagnetic pulse can lead to production of particles such as dilepton pairs or pions, or to nuclear excitations which may be otherwise inaccessible.

In particular, electromagnetic excitation of modes based on the nuclear giant dipole resonance (GDR) may lead to very exotic final states[1,2] in which neutrons oscillate against protons with a very large amplitude. The existence and decay mechanisms of such states is unknown at present. However, this electromagnetic process efficiently excites collective states so that little or no temperature is produced during the very short time scale (of order 1 fm/c) of the collision. One may thus hope to use this type of reaction to search for fragile, weakly bound exotic states such as multineutron clusters which might be formed in the decay of the possibly strongly excited multi-GDR states.

Experimentally, the electromagnetic dissociation of a projectile or target nucleus in peripheral collisions at relativistic energies has been studied in a variety of ways. The investigation of the interaction of ^{16}O and ^{28}Si projectiles with plastic foil detectors[3–5] at the AGS and CERN has provided information on the total charge-changing cross sections. Cross sections for the removal of single nucleons from the target,[6–8] and projectile[9] nucleus have been studied using activation methods. First results are now available from the E814 collaboration[1] at the AGS where cross sections were, for the first time, measured for the decay of electromagnetically excited projectiles into a wide range of exclusive and semi-inclusive channels.[10]

In the present paper we will develop a framework for quantitative analysis of such data, based on the method of virtual quanta. In particular, emphasis is placed on using as much available information as possible on experimental photoabsorption cross sections to obtain realistic values for the excitation energy distributions for single and multiple excitations. Furthermore, to provide some information on whether or not a particular decay mode experimentally observed is "exotic," we calculate the decay of the electromagnetically excited projectile or target under the assumption that complete mixing into the compound nucleus takes place, i.e., by using the standard statistical model for the nuclear decay probabilities.

The basic framework for such calculations has been developed elsewhere.[11,12] We will briefly outline the method for calculating excitation probabilities in Sec. II with emphasis on differences to previous work and describe there our results for multiple excitation and delineate our approach to incorporate statistical decay. Section III will provide a comparison with some of the experimental data available to date and contain strategies to optimize searches for rare decay products from such states. Section IV contains the summary and conclusions.

II. THEORETICAL FRAMEWORK

A. Outline of methods

The framework for the analysis of the electromagnetic excitation of nuclei in peripheral collisions, and their subsequent decay, is described below. The approach is based on the equivalent photon method, or Weizsäcker-Williams approximation[13–16] combined with the assumption that the nuclei move along straight trajectories. Quantum interference effects are thereby neglected but otherwise the approach is quite general in nature and can be applied whenever the nuclei are relativistic. Similar, although more schematic, methods have been used in Refs. 17–21. For convenience, we restrict ourselves to

the excitation of the projectile by a stationary target, but target and projectile can, of course, be interchanged. The collision is viewed in the rest frame of the projectile.

The description of a large impact parameter interaction involves the folding of the equivalent photon number spectrum generated by the target with the appropriate nuclear photoabsorption cross section. The equivalent photon spectra are obtained following Bertulani and Baur[20,21] and depend on the projectile energy and impact parameter as well as on target charge number. In general, they differ for different values of the parity and angular momentum of the electromagnetic multipole field. However, as the Lorentz boost of the projectile γ_P approaches ∞, all number spectra become equal to that for the pure $E1$ mode.[17] Since all nuclear photoabsorption cross section are strongly dominated by $E1$ absorption, the overwhelming part of the cross section will be given by $E1$ mode and excitations with higher electric multipolarities, such as $E2$, and all magnetic multipoles can be safely neglected at highly relativistic energies.

We assume that the impact parameter is large enough so that the target charge distribution as seen by the projectile can be treated as a point charge. Corrections to such an assumption for closer collisions are discussed below. The number of photons per unit area at an energy E_γ and impact parameter b that replace the electromagnetic field of the target is given by[22]

$$\mathcal{N}(E_\gamma,b)=\frac{1}{E_\gamma}\left[\frac{Z_T^2\alpha}{\pi^2\beta_P^2 b^2}\right]\left[x^2K_1^2(x)+\frac{x^2}{\gamma_P^2}K_0^2(x)\right], \quad (1)$$

where

$$x=\frac{E_\gamma b}{\gamma_P\beta_P\hbar c}. \quad (2)$$

Here, α is the fine structure constant, $\beta_P c$ is the projectile velocity, the target charge is Z_T, and the argument of the modified Bessel functions, K_0 and K_1, is the dimensionless adiabaticity parameter x. The impact parameter b can assume any value greater than some minimum, $b_{\min}$, to be specified later, above which the interaction is dominated by the electromagnetic field. For E_γ or b exceeding critical values, such that $x>1$, the above spectrum decays exponentially. This implies that the maximum energy reachable by electromagnetic excitation is approximately $E_\gamma^{\max}=197\gamma_P/b_{\min}$. Furthermore, this cutoff insures convergence of the impact parameter and energy integrations necessary to obtain cross sections (see below).

The Weizsäcker-Williams approximation implies that the virtual photon flux can be treated as a flux of real photons and that there be no interference effects between these photons. This approximation has been described in detail in Refs. 16 and 17; at relativistic energies it is very accurate.

The point-charge approximation made to obtain Eq. (1) is correct as long as b is large enough so that the nuclear charge distributions do not overlap. In practice, we take $b_{\min}=R_T+R_P$, where $R_{P,T}=(1.2\text{fm})\cdot A_{P,T}^{1/3}$, despite the fact that for such a choice the nuclear surfaces may have some, albeit small, overlap.

The influence of this overlap on the virtual photon spectrum can be estimated by noting that the Coulomb potential for a target with a spherical charge distribution at a distance r from the center is

$$V_C(r)=\frac{Z_T(r)e^2}{r}, \quad (3)$$

where $Z_T(r)e$ is the total charge inside a sphere with radius r. The effective charge of the target therefore obviously depends on the impact parameter. The influence of this modified charge on the virtual photon spectrum, however, is fairly small.

We have estimated the change in virtual photon flux due to the finite charge distribution of the target in the following way. Taking charge distributions as determined by electron scattering,[23] numerical integration of a Woods-Saxon potential was performed over the target nucleus. The collisions most sensitive to the finite size of the target nucleus are those for which $b\sim b_{\min}$, where some portion of the target charge, Z_T, is screened from the projectile, This impact parameter dependent effective target charge can be used to estimate the change in the equivalent photon spectrum due to the finite size of the target nucleus. Averaging the flux over the size of the projectile, the change in the photon flux so calculated is less than 3%. Thus, in all calculations shown below, the finite size of the source was not included, especially in view of the fact that this correction is comparable to the uncertainty introduced by the choice of $b_{\min}$.

The nuclear photoabsorption cross section σ_γ to be folded with the equivalent photon spectrum is taken from the literature.[24–26] It has been accurately measured in the energy range from $E_\gamma^{\min}\sim 10$ MeV to several GeV in energy. Experimental values for the photoabsorption

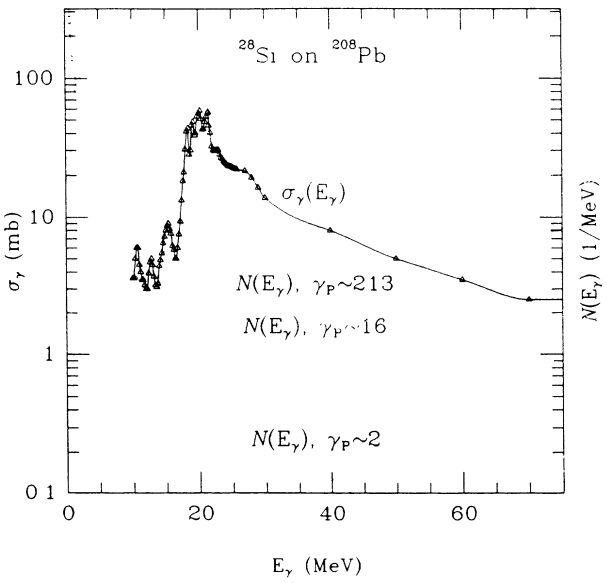

FIG. 1. The photoabsorption cross section from Ref. 25 for a ^{28}Si projectile and the integrated virtual photon spectrum of a ^{208}Pb target moving with Bevalac, AGS, and SPS energies through the rest frame of the projectile.

cross section for the ^{28}Si nucleus are shown in Fig. 1. Also shown in this figure are equivalent photon number spectra for various beam energies in Si-Pb collisions and integrated over impact parameter. Note that the virtual photon flux, deduced from Eq. (1), near the GDR as seen by the Si nucleus passing by the Pb target is of order 10^{46}/(MeV cm^2 s), with which typical luminosities of real-photon beams should be compared.

Since we are only interested in excitations beyond the particle decay thresholds (which are greater than 10 MeV for the nuclei of interest here) the photoabsorption cross sections are set to zero below a minimum photon energy $E_\gamma^{\min}$ of 10 MeV. In any event, the cross section for the absorption of $E1$ photons with $E_\gamma < 10$ MeV is very small,[27] so that their contribution to the excitation of the high-lying states of interest here can be neglected.

The projectile can then be excited by the absorption of one or more of the virtual photons from the target. The total excitation energy of the nucleus E^* resulting from the excitation process is the sum of the individual energies of the photons absorbed. Each photon can carry any energy between 10 MeV and E^*, with the constraint that the sum of the photon energies reproduces the excitation energy.

Implicit in the above structure is the assumption that the photoabsorption to all orders occurs in the ground state of the projectile. Such an assumption is reasonable, as the time interval $\Delta t = 2R_T/\gamma_P c \sim 1$ fm/c, over which the projectile moves through the target's equivalent photon field, is an order of magnitude less than typical nuclear equilibration times. The effect of finite nuclear temperatures on the absorption cross section[28] is thus neglected altogether, consistent with the use of the experimentally measured photoabsorption spectra.

Within our classical approach the probability densities for the multiple excitation cross sections are constructed by repeated folding of the probability for the absorption of single photons at a fixed impact parameter b. The differential cross section for the nth-order process is then the result of the integration over all impact parameters contributing to the process.

The mean number of photons absorbed by the projectile during a collision at impact parameter b is given by

$$m_\gamma(b) = \int dE_\gamma \mathcal{N}(E_\gamma,b)\sigma_\gamma(E_\gamma) = \int dE_\gamma \Phi(E_\gamma,b) \ . \quad (4)$$

The redefinition of the integrand above is done for the purposes of clarity in the equations to follow.

The integral above is performed from $E_\gamma^{\min}$ to excitation energies safely above the adiabatic cutoff defined by the beam energy and impact parameter. The mean number of absorbed photons so obtained is shown in Fig. 2 for ^{28}Si and ^{32}S induced collisions at 14.6 and 200 GeV/nucleon, respectively. The absorption cross sections for ^{28}Si and ^{32}S are similar, so the difference in the two curves is a result of the fact that the energy integrated number spectrum, in addition to depending on the square of the target charge, increases logarithmically with projectile energy.

The excitation process is viewed as the single or multiple excitation of a classical harmonic oscillator. In this

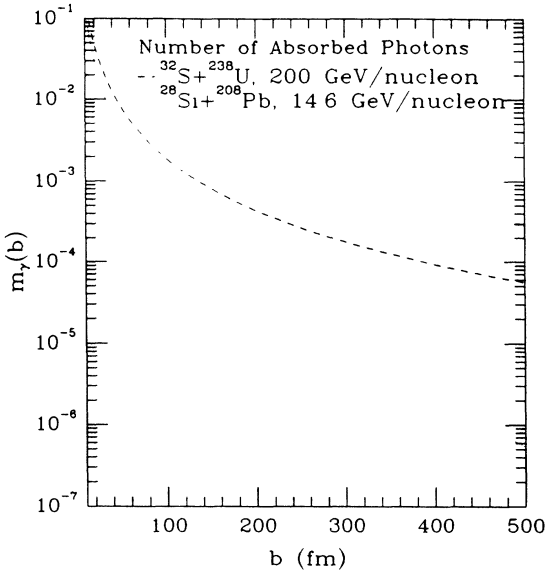

FIG. 2. The mean number m_γ of absorbed photons for collisions with impact parameter b.

harmonic approximation, the excitation probability for the nth-order process is given by a Poisson distribution in the probability for the single-step process.[11] This fact has been exploited by others[18,20] for the investigation of multistep processes.

Thus, the probability for the absorption of a single photon, of any energy, during a collision at impact parameter b is given by

$$\mathcal{P}^{(1)}(b) = m_\gamma(b) e^{-m_\gamma(b)} \ , \quad (5)$$

For a trajectory at an impact parameter b, the properly normalized probability density that the photon absorbed by the projectile has an energy E is then given by

$$q^{(1)}(E_\gamma,b) = \frac{\Phi(E_\gamma,b)}{m_\gamma(b)} \ . \quad (6)$$

All of the details necessary for the calculation of the first-order cross section are contained in Eqs. (5) and (6). The overall probability for the single-step process is then simply the product of the probability density for absorption of a single photon and the probability density that this photon carries an energy E.

The differential cross section for the absorption of exactly one photon, leading to an excitation energy E^*, is therefore given by

$$\frac{d\sigma^{(1)}}{dE^*} = \int db \, 2\pi b \mathcal{P}^{(1)}(b) q^{(1)}(E^*,b) \ , \quad (7)$$

or

$$\frac{d\sigma^{(1)}}{dE^*} = \int db \, 2\pi b e^{-m_\gamma(b)} \Phi(E^*,b) \ . \quad (8)$$

The probability density that two photons at impact parameter b are absorbed is

$$\mathcal{P}^{(2)}(b)=\frac{m_\gamma^2(b)}{2!}e^{-m_\gamma(b)}, \tag{9}$$

while the probability density for the absorption of two photons leading to an excitation energy E^* is

$$q^{(2)}(E^*,b)=\frac{\int dE_1\Phi(E_1,b)\Phi(E^*-E_1,b)}{m_\gamma^2(b)}. \tag{10}$$

The cross section for the transfer of exactly two photons is then

$$\frac{d\sigma^{(2)}}{dE^*}=\int db\,2\pi b\mathcal{P}^{(2)}(b)q^{(2)}(E^*,b), \tag{11}$$

or

$$\frac{d\sigma^{(2)}}{dE^*}=\frac{1}{2!}\int db\,2\pi b e^{-m_\gamma(b)}\times\int dE_1\Phi(E_1,b)\Phi(E^*-E_1,b). \tag{12}$$

The differential cross section for the excitation of the projectile by the transfer of exactly n photons is, finally,

$$\frac{d\sigma^{(n)}}{dE^*}=\frac{1}{n!}\int db\,2\pi b e^{-m_\gamma(b)}\int dE_1\cdots dE_{n-1}\Phi(E_1,b)\cdots\Phi(E^*-E_1-\cdots-E_{n-1},b), \tag{13}$$

and the total excitation cross section to any order is given by

$$\sigma=\int dE^*\left[\frac{d\sigma^{(1)}}{dE^*}+\frac{d\sigma^{(2)}}{dE^*}+\frac{d\sigma^{(3)}}{dE^*}+\cdots\right]. \tag{14}$$

The integrals above are performed numerically by Gaussian quadrature. Considerable care is required in order to obtain accurate results. The fourth-order total excitation cross section, for example, requires *five* nested integrations, three over individual photon energies and one each over the excitation energy and impact parameter. Each integral extends over a wide range of values, while the fold integrals over the photon energies need to be carried out with a density of points sufficient to integrate accurately the fine structure of the photoabsorption cross section in the GDR region. Stable results from the numerical method involved double precision arithmetic and up to 100-point integration, requiring considerable CPU time.

In order to test our numerical procedures we have compared results from the present approach to predictions based on the schematic method, e.g., Ref. 20, where a delta function for the GDR strength distribution is assumed. To make this comparison we chose the input parameters, i.e., the projectile energy, $E_{\rm proj}$, and the photoabsorption cross section, σ_γ, so as to reproduce the assumptions of the schematic method. A Gaussian photoabsorption cross section of very small ($\ll 1$ MeV) width and total area reproducing the classical sum rule was generated, centered at an energy of $80/A^{1/3}$ MeV.

The results of this comparison are shown in Table I. The results from the schematic method are labeled σ (Ref. 20); the results we obtain with the narrow Gaussian photoabsorption cross section are labeled $\sigma(\sigma_\gamma^G)$. The cross sections obtained under these assumptions are in good agreement, to all orders of excitation studied, with the previous results of Ref. 20.

The third column in Table I, labeled $\sigma(\sigma_\gamma^{\rm exp})$, contains the results obtained by integration over the experimental photoabsorption cross section up to 500 MeV. The contribution to the total excitation cross sections from processes other than GDR excitation is apparent.

B. Excitation cross sections

In this section, we present results obtained with the method discussed above, focusing on single-step and multistep excitation probabilities and cross sections. The energy dependence of the differential cross sections for the excitation of the ^{28}Si projectile to first, second, and third order is shown in Fig. 3 for collisions with a ^{208}Pb target at AGS energies ($E_{\rm lab}/A=14.6$ GeV). Note the importance of the asymmetric line shape and the reappearance of the fine structure of the GDR in ^{28}Si in the multiple excitation cross sections. The peaks in the cross sections of order n appear close to an excitation energy of $E^*=nE_{\rm GDR}$, as expected. However, due to the very asymmetric shape of the photoabsorption cross section at higher energies,[29] the widths, $\Gamma(n)$, are approximately $\Gamma(n)=\frac{3}{2}n\Gamma_{\rm GDR}$, i.e., significantly bigger than what is obtained by folding Lorentzians [note that folding Lorentzian photoabsorption cross sections give $\Gamma(n)=n\Gamma_{\rm GDR}$, while folding Gaussians give $\Gamma(n)=\sqrt{n}\,\Gamma_{\rm GDR}$].

The multistep excitation cross sections, shown in Fig. 3, are small compared to that for the single-step absorp-

TABLE I. The total excitation cross sections calculated following Ref. 20, and those from this work: $\sigma(\sigma_\gamma^G)$ is calculated using a very narrow Gaussian to describe the photoabsorption probability and $\sigma(\sigma_\gamma^{\rm expt})$ using the experimental photoabsorption cross section.

Order	σ (Ref. 20)	$\sigma(\sigma_\gamma^G)$	$\sigma(\sigma_\gamma^{\rm expt})$
	^{16}O on ^{238}U at 100 GeV/nucleon		
1	N/A	1.03 b	2.5 b
2	3.1 mb	3.16 mb	20.6 mb
3	22 μb	22.9 μb	328 μb
4	160 nb	164.3 nb	4.8 μb
	^{32}S on ^{238}U at 100 GeV/nucleon		
1	N/A	2.63 b	4.3 b
2	17 mb	17.5 mb	46.3 mb
3	250 μb	273 μb	1.1 mb
4	4 μb	4.3 μb	26.6 μb

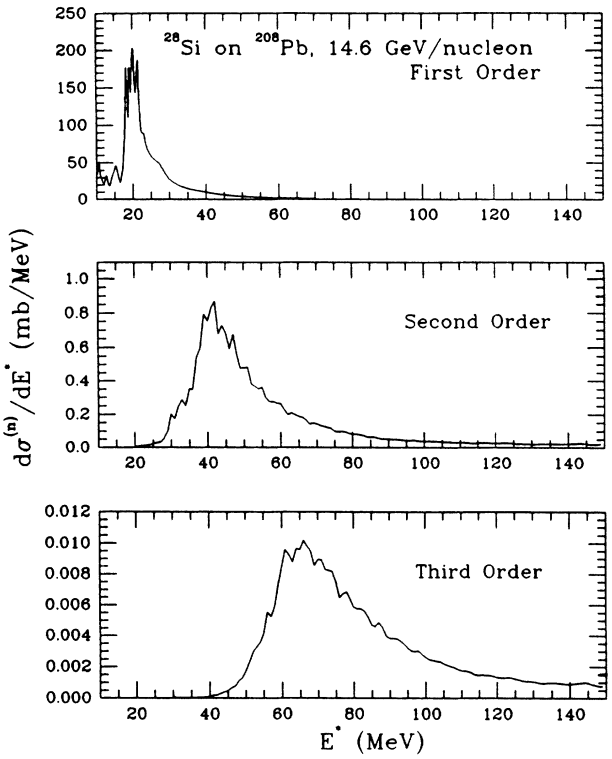

FIG. 3. The total differential Coulomb excitation cross sections for ^{28}Si on ^{208}Pb at $E_{lab}/A = 14.6$ GeV for the first-, second-, and third-order processes.

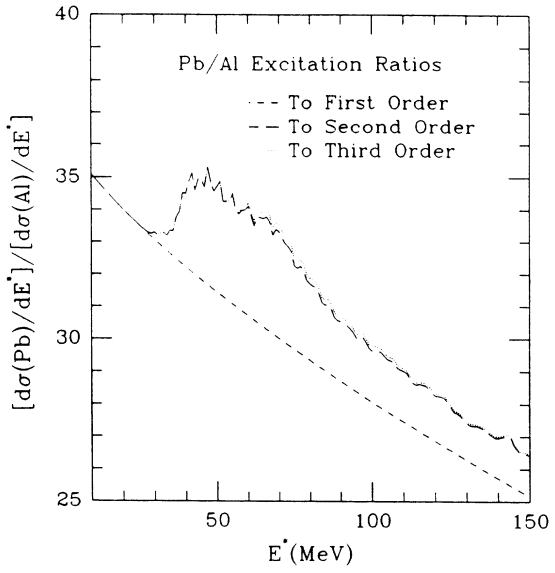

FIG. 4. The ratio of the differential Coulomb excitation cross sections for ^{28}Si on ^{27}Al and ^{208}Pb targets as a function of the excitation energy.

tion to the same excitation energy via the quasideuteron process.[29] This implies that structures in the excitation energy spectrum due to multiple GDR excitation will be very difficult to find experimentally. Detection of such structures will require sophisticated techniques, including exclusive studies of decay processes.

One possibility is to look for signatures in the ratio of the differential excitation cross section for two targets with very different charge numbers. Higher-order excitations will be enhanced in this ratio because the number spectrum, Eq. (1), scales like Z_T^2, while the nth-order cross section behaves approximately like Z_T^{2n}. Note, however, that even for the first-order process the ratio will not be independent of beam energy and excitation energy, but decreases slightly, as the number spectra for the two targets sample different ranges of impact parameter.

Predictions for the ratio of differential cross sections, for a 14.6 GeV/nucleon ^{28}Si projectile on a ^{208}Pb target and a ^{27}Al target, are shown in Fig. 4. The structure due to the double excitation of the GDR in ^{28}Si is clearly visible in this spectrum above an excitation energy of 40 MeV. However, the enhancement above the smooth (quasideuteron) background is only about 10%, so very careful measurements are necessary to establish such an excitation.

The ratio of the second-to first-order cross sections varies from up to 10% at AGS energies, to less than 5% at CERN energies. The reason for this decrease is visible in Fig. 5, where the dependence of the total excitation cross sections on the projectile kinetic energy are shown. In this figure, we plot results for multiple excitation cross sections integrated over all excitation energies and for multiple GDR excitation only (defined by zeroing the photoabsorption cross section below $E_\gamma = 18$ MeV, and above $E_\gamma = 36$ MeV; this interval contains one classical $E1$ sum rule of $60 N_P Z_P / A_P$ mb MeV). Although the photon number spectrum extends to much higher ener-

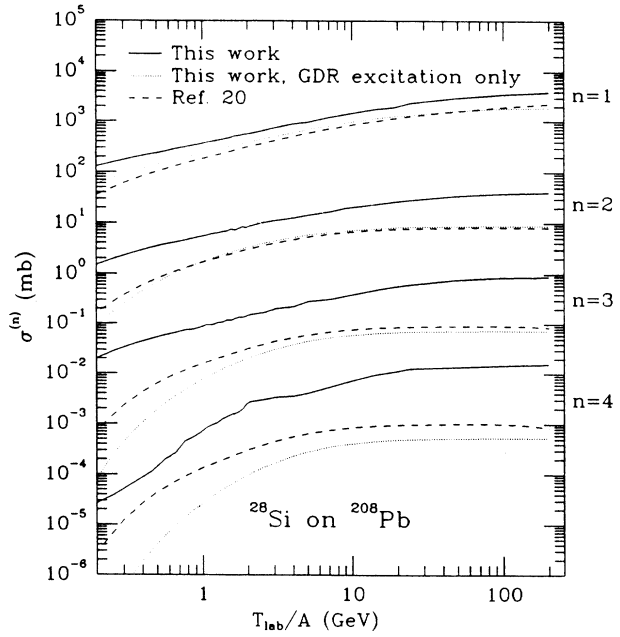

FIG. 5. The total excitation cross sections from the schematic method (Ref. 20, dashed line), and from this work (solid line), as a function of the projectile kinetic energy. Also shown, the total cross sections by integration over only the GDR (dotted line).

gies at ultrarelativistic projectile energies, the multiple excitation cross sections, and, in particular, multiple GDR excitation, do not depend strongly on the beam energy as soon as $E_\gamma^{\max} \sim 197\gamma_P\beta_P/b_{\min}$ exceeds the GDR resonance energy. For ^{28}Si, $E_{\rm GDR}$ is 20–25 MeV, corresponding to $\gamma_P \sim 2$.

This saturation is due to the impact parameter dependence of the excitation cross sections. The integral over impact parameter for the first-order process increases like $\ln(\gamma_P)$ while all higher-order cross sections are, above $E_{\rm lab}/A \sim 10$ GeV, only very weakly dependent on the beam energy (see Fig. 5). This is relevant for the determination of the optimal beam energy for the study of multiple excitation processes, as discussed below.

C. Comparison to other methods

Multiple Coulomb excitation cross sections at relativistic energies have been investigated previously with standard semiclassical[11,12] and classical[17,21] methods. These calculations were intended to give estimates for the relative importance of higher-order processes. However, these authors neglect important aspects of the projectile photoabsorption in that they assume, for example, that the GDR strength is a delta function centered at an energy of $80/A^{1/3}$ MeV, with strength parameter equal to 100% of the energy weighted sum rule. This restricts all absorbed photons to have energy $E_\gamma = E_{\rm GDR}$.

The comparison of the total excitation cross sections from the schematic method, labeled σ (Ref. 20) with calculations using the experimental photoabsorption cross section, labeled $\sigma(\sigma_\gamma^{\rm exp})$, are shown in Table I. The effect that the region of the photoabsorption cross section not included in the GDR has on the total cross section is obvious. The integrals of our differential cross sections over the GDR region alone are similar to those by the schematic method, as visible in Fig. 5, but the contribution from quasideuteron absorption and absorption of even higher-energy photons ($E_\gamma^{\max} \sim 197\gamma_P/b_{\min}$) to the total cross section is very important at other excitation energies.

In any collision resulting in electromagnetic excitation, higher-order processes compete with single-step excitation. The high-energy tail of the photoabsorption cross section (see Fig. 1) leads to the dominance of the first-order process, over that for the higher orders, at any excitation energy. In Fig. 3, the excitation cross section at $E^* = 40$ MeV, approximately the maximum of the double-excitation cross section, is ~ 10 mb, with less than a 10% contribution from second-order excitation. The contribution from the first-order process is, of course, neglected in the schematic model, where only photons with $E = E_{\rm GDR}$ are absorbed.

The investigation of the dependence of the multiple excitation process on the beam energy reveals that the relative magnitude or higher-order processes is largest at relatively small projectile energies. To make this point quantitative, we show, in Fig. 6, the ratio $\sigma_{\rm GDR}^{(n)}/\sigma_{\rm GDR}^{(1)}$, where the cross section $\sigma_{\rm GDR}^{(n)}$ implies that only photons with energies in the range 18–36 MeV, i.e., the GDR region, are used in the folding procedure. This ratio exhibits broad maxima at projectile kinetic energies $T_{\rm lab}$ of approximately 2, 5, and 8 GeV/nucleon for second, third, and fourth order, respectively.

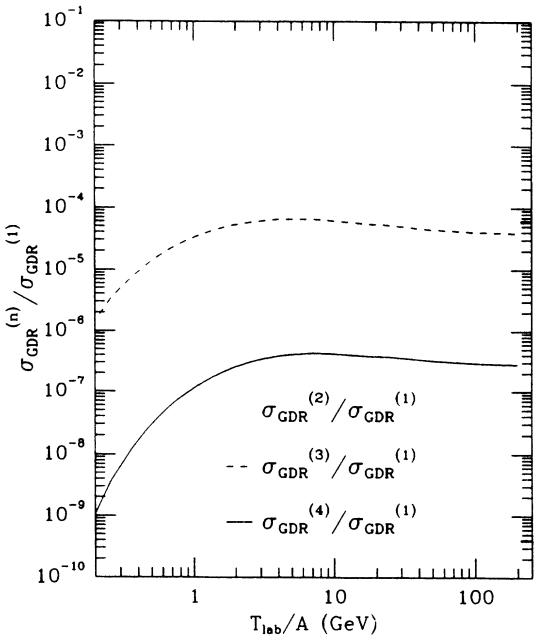

FIG. 6. The ratios of the nth-order GDR excitation cross sections to the first-order GDR cross section as a function of the projectile kinetic energy.

It is therefore more important for the experimental isolation of higher-order processes to determine the relative importance of the n-fold GDR excitation cross section to the total excitation cross section in the same energy range. To make this comparison, we define the ratio $\sigma_{\rm GDR}^{(n)}/\sigma_n^{(1)}$, where $\sigma_{\rm GDR}^{(n)}$ is the nth-order GDR excitation cross section. The quantity $\sigma_n^{(1)}$ is defined as the integral of the first-order cross section over the energy interval covered by the nth-order GDR excitation process. In Fig. 7, this ratio is shown for $n = 2, 3$, and 4, as a function of the projectile kinetic energy.

Taking the results from Figs. 6 and 7, one may deduce an optimal beam energy for the investigation of the nth-order GDR excitation. The most promising strategy then seems to involve the choice of a beam energy at or slightly below the appropriate maximum visible in Fig. 6. Such a choice minimizes the "noise" contribution from the first-order excitation, while at the same time providing reasonable event rates.

D. The statistical decay

Single and multiple GDR excitation leads to particle unstable states, i.e., to dissociation of the projectile (or target), so a complete description of these processes should also include the fragmentation probabilities. As discussed above, the main interest in studying such excitations is the search for collective effects in the decay of such states, possibly induced by the large amplitude collective motion of neutrons versus protons following mul-

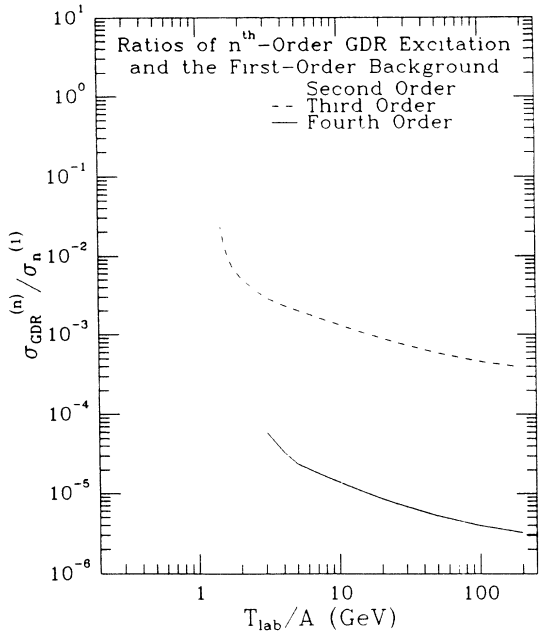

FIG. 7. The ratios of the nth-order GDR cross section, $\sigma_{\mathrm{GDR}}^{(n)}$ and the integral of the total first-order cross section over the same excitation energy range, $\sigma_n^{(1)}$, as a function of projectile kinetic energy.

tiple GDR excitation. In order to be able to determine the collectivity of a particular decay mode, it is therefore very important to provide quantitative information on decay probabilities assuming no collectivity.

The picture we assume for this background process is that the states excited through (multiple) GDR excitation mix completely with the underlying compound nuclear states of the projectile or target and subsequently decay statistically. To treat the statistical decay and to make specific predictions for probabilities for different decay channels we use the standard nuclear statistical model and perform decay calculations with the computer code CASCADE.[30]

This code was developed for the simulation of the decay of compound nuclei produced in heavy-ion fusion reactions, but the decay probabilities are independent of the formation process. In the present case, the projectile is excited electromagnetically, to an energy given by the sum of the energies of the absorbed photons.

We further assume that all excited states have spin/parity of $J^{\pi}=1^{-}$, appropriate for $E1$ excitation. Multiple $E1$ excitation can lead to states of other spins and parities, of course, but for the excitation energies of interest here, all such states are very far from the yrast line. Therefore, these spin values and parities do not significantly influence the decay probabilities presented here. Furthermore, as shown above, higher-order excitations are always a small fraction of the total excitation cross section.

The program CASCADE is used to compute the partial strengths $\mathcal{T}_y$ into all possible decay channels, labeled by y, of a statistically equilibrated nucleus at an excitation energy E^*. This leads to a total fragmentation cross section for the channel y of

$$\sigma_y = \int dE^* \mathcal{T}_y(E^*) \left[\frac{d\sigma^{(1)}}{dE^*} + \frac{d\sigma^{(2)}}{dE^*} + \cdots \right] . \quad (15)$$

The parameters entering the statistical model calculations were the default values described in Ref. 30. These parameters have been extensively tested in the study of heavy-ion-induced evaporation residue cross sections and should lead to a realistic description of statistical decay probabilities in the excitation energy range between 20 and 150 MeV.

Implicit in our assumption of complete mixing is also the neglection of any isospin considerations for the calculation of the decay probabilities. Single-photon absorption by an isospin $I=0$ nucleus into the GDR leads to a state of pure isospin $I=1$. Isospin conservation would then severely suppress, e.g., the $^{28}\mathrm{Si}\rightarrow{}^{24}\mathrm{Mg}+\alpha$ decay to the low-lying states as the density of $I=1$ levels in ^{24}Mg is very small compared to the density of $I=0$ levels at low excitation energies.

The probabilities for single-proton and single-neutron evaporation are also dependent on isospin, although to a lesser degree than the α channel. Isospin conservation would imply that the $1n$ and $1p$ decay probabilities are equal, except for the Coulomb barrier penetrability and the different separation energies for the two nucleons which, on balance, lead to an increased proton evaporation probability in light nuclei. Incidentally, increasing

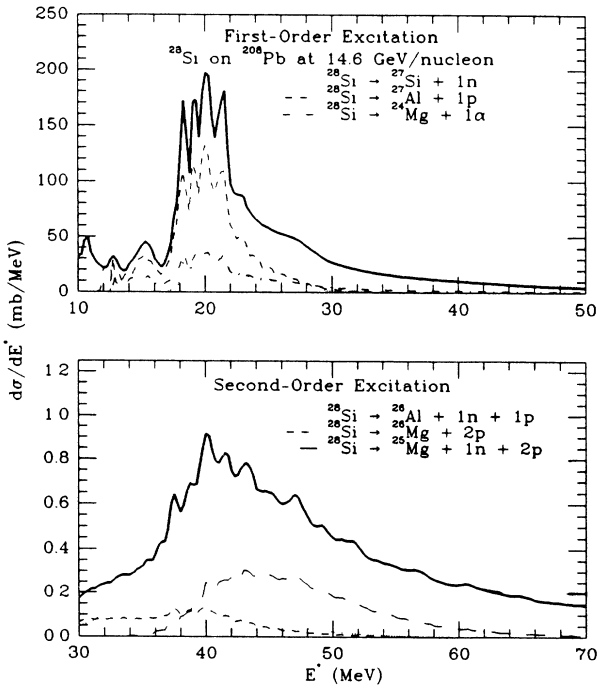

FIG. 8. The differential first-order (top plot, solid line) and second-order (bottom plot, solid line) excitation cross sections versus the excitation energy. The dashed lines indicate the contributions from the important decay channels, labeled in the appropriate figure.

the degree to which the $I=0$ state is mixed with the $I=1$ GDR state before the decay would further enhance the proton channel at the expense of the neutron branch.

However, our main motivation is not to describe decays of the GDR state in the projectile. These decays are known[31–33] to contain nonstatistical components at the 20% level and indeed are sensitive to the degree of isospin mixing of the GDR state.[32] Rather, we focus on the decays of higher excited states (such as those following multiple GDR excitation) where isospin considerations are presumably much less important.

The calculated differential excitation cross sections for the first- and second-order processes, and the differential cross sections for the dominant decay channels for these processes, are shown in Fig. 8. The $1n$, $1p$, and 1α channels dominate the decay of the GDR excited in the single-step process, but more complex fragmentation channels contribute for excitation energies reached during multistep excitation. Note the strong dependence on excitation energy for the various fragmentation processes.

III. RESULTS AND COMPARISON WITH EXPERIMENTAL DATA

In this section we would like to compare predictions from our model with some of the data which recently became available for electromagnetic dissociation of relativistic projectiles. We will focus on results from the E814 collaboration as they provide the only exclusive cross sections for identified final channels.

These experimental results, as well as a detailed description of the techniques and apparatus used to collect the data, have recently been published elsewhere.[10] The experiment was performed, in part, to investigate the electromagnetic dissociation of 14.6 GeV/nucleon ^{28}Si nuclei by ^{27}Al, ^{120}Sn, and ^{208}Pb targets. We will show only the final experimental results here and direct the reader to Ref. 10 for the experimental aspects of the measurements.

It is important to remember that the use of the statistical model to describe the decay of light, self-conjugate, nuclei such as ^{28}Si is not necessarily correct for all channels. In particular, the $1n$, $1p$, and 1α channels are especially susceptible to the direct decay mechanism and isospin considerations, as discussed above, so quantitative agreement between this calculation and the experimental data should not be expected for these channels. However, it is interesting to compare our predictions for more complex decay channels with the data as they should provide a benchmark for whether or not these decays are statistical in nature.

The experimental data are shown in Table II, along with our predictions for electromagnetic excitation followed by statistical decay. These results are also plotted versus the calculated threshold Q value for each decay channel in Fig. 9. The approximate exponential falloff of the partial cross sections with the excitation energy, or the threshold Q value, is quite well reproduced by the calculation. The agreement is fairly quantitative for all channels, although channels involving the emission of protons are generally somewhat overestimated while neutron decay probabilities are underestimated. The largest difference between the experimental data and the calculation, a factor of 3, occurs in the $2p$ and $2n$ channels. Whether this discrepancy is due to the neglect of specific nuclear structure effects such as incomplete isospin mixing, or may already be an indication of exotic decay mechanisms, is an interesting but open question.

Overall, one should stress that the present calculation does not make use of any adjustable parameters. The parameters for the statistical model calculations were taken from the literature.[34–37] The electromagnetic excitation probabilities are calculated in an essentially parameter-free way, since the nuclear photoabsorption cross sections were taken from experiment. In view of this, the agreement obtained is quite impressive.

For the relatively low excitation energies experimentally studied up to now, the trend of the data quite closely follows what is expected from first-order excitation followed by statistical decay. In particular, the fact that all other parameters are externally determined implies that the Weizsäcker-Williams number spectrum, Eq. (1), correctly describes the photon flux.

Higher-order processes do not provide a significant contribution to the results of the calculations reported in Table II and Fig. 9. As mentioned above, a promising in-

TABLE II. The exclusive cross sections measured by E814, and the results calculated in the present approach, for the electromagnetic dissociation of ^{28}Si at $E_{\rm lab}/A=14.6$ GeV/nucleon. All cross sections are in mb, while the threshold Q value for each channel is in MeV.

	^{27}Al target		^{120}Sn target		^{208}Pb target		
Channel	$\sigma_{\rm meas}$	$\sigma_{\rm calc}$	$\sigma_{\rm meas}$	$\sigma_{\rm calc}$	$\sigma_{\rm meas}$	$\sigma_{\rm calc}$	$-Q$
$1n+^{27}$Si	10.8±2.8	5.39	101.9±8.2	70.49	263.5±15	177.66	17.2
$1p+^{27}$Al	34.2±4.7	21.62	290.6±13	283.96	672.2±25	717.13	11.6
$2n+^{26}$Si	0.4±0.2	0.03	1.3±0.5	0.34	3.2±0.9	0.83	30.5
$1n1p+^{26}$Al	2.3±1.9	2.79	21.0±4.9	35.60	67.3±8.9	88.50	24.6
$2p+^{26}$Mg	3.2±0.8	4.74	21.4±2.2	61.21	55.6±3.7	153.03	19.9
$2n1p+^{25}$Al	0.4±0.5	0.13	1.6±0.6	1.55	3.6±1.0	3.79	36.0
$1n2p+^{25}$Mg	1.86±1.3	1.41	13.2±3.4	17.63	16.6±5.2	43.30	30.1
$2n2p+^{24}$Mg	0.3±0.3	0.21	3.6±0.7	2.59	3.6±1.1	6.27	38.3
$\alpha+^{24}$Mg		10.00		130.45		334.66	10.0

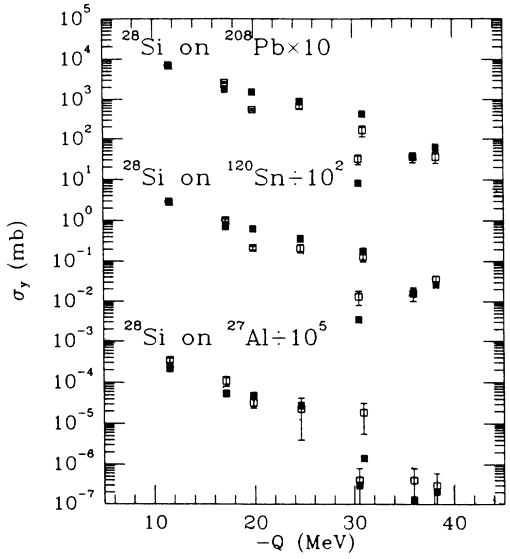

FIG. 9. Comparison of E814 data, Ref. 10, for the electromagnetic dissociation of ^{28}Si at $E_{lab}/A = 14.6$ GeV/nucleon (open squares with error bars), and the present calculation (solid squares) for all measured decay channels and targets. The dotted line is a pure exponential and is included to guide the eye.

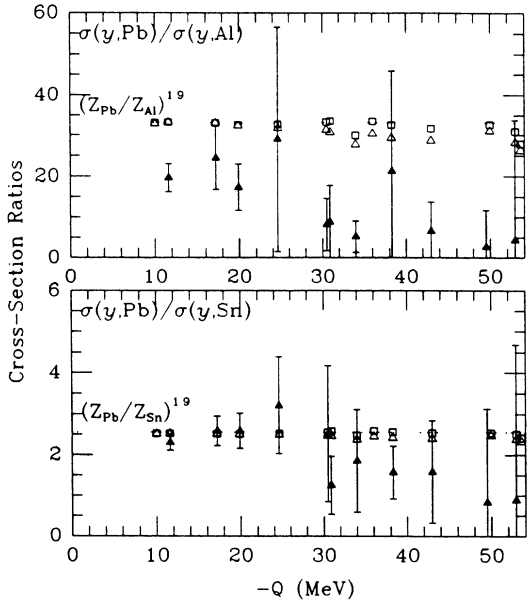

FIG. 10. The ratios of the E814 cross sections, Ref. 10, for the electromagnetic dissociation of 14.6 GeV/nucleon ^{28}Si projectiles (solid points), the calculated ratios to first order (open triangles) and to third order (open squares). The dotted line gives the ratio expected for first-order excitation.

dicator of higher-order processes comes in the ratio of cross sections for different targets. For first-order electromagnetic excitation, one would naively expect that the ratio of cross sections for two different targets would be on the order of the ratio of the square of the target charges $(Z_{T1}/Z_{T2})^2$. The exponent is actually closer to 1.9, due to the different ranges of impact parameter b sampled for the two targets. If it were possible to select the events in which exactly n photons were absorbed, the excitation cross section for these events would behave like $Z_T^{1.9n}$. Thus, a definite indication of the multiphoton process would involve a ratio of cross sections larger than $(Z_{T1}/Z_{T2})^{1.9}$.

The cross-section ratios from the E814 data are given in Fig. 10, as the triangles with the error bars. The calculated ratios are shown as the open symbols, results of the calculation to first order are given by the triangles and to third order by the squares. The upper plot gives the experimental ratios of the cross sections for a 14.6 GeV/nucleon ^{28}Si projectile on a ^{208}Pb target to that for a ^{27}Al target, as a function of the calculated threshold Q value. The lower plot gives the ratios for ^{208}Pb and ^{120}Sn targets.

The fact that the experimental ratio for the ^{208}Pb$-^{27}$Al targets falls well below the expected behavior is probably an indication of some contributions, for the lighter target, of nonelectromagnetic processes to the projectile excitation. The experimental ratios are much closer to those expected for Coulomb excitation for the ^{208}Pb/^{120}Sn targets, implying that the experimental selection of electromagnetic dissociation events was more accurate for these targets, as discussed in Ref. 10.

The expected enhancement of some of the cross-section ratios, when including calculations up to third order, is visible in Fig. 10 for channels for which $|Q| > 30$ MeV. These are the $3p$, $2n+1p$, $2n+2p$, and $1n+3p$ channels, which will serve as the most sensitive indicators for the second- and third-order processes.

Obviously, the uncertainties in the ratios of the experimental data of Ref. 10 are presently far too large to isolate the multistep process from such ratios. An experimental uncertainty in the ratios of less than about 5% is necessary before any measurement of the multistep process is possible.

The exponential decline of the partial cross sections with the threshold Q value, seen in Fig. 9, continues within this model to higher values of Q. This would provide an estimate for the cross sections one might expect for completely statistical decay of the ^{28}Si projectile into the $3n$ and $4n$ channels.

According to our assumption, in which the GDR mixes completely into the compound nucleus before decaying, the partial cross section for the $^{28}\text{Si}\rightarrow{}^{24}\text{Si}+4n$ channel is less than 1 pb, which is clearly not presently measurable. This is a result of the very negative threshold Q value of -64.5 MeV for this channel, coupled with the fact that sequential statistical emission of four neutrons from ^{28}Si is highly unlikely. Reaching $E^*=65$ MeV by multiple absorption of GDR photons requires at least third-order excitation. Thus, a striking experimental signature of the higher-order processes would be a dramatic enhancement of the $4n$ partial cross section from ^{28}Si over that resulting from the assumption of complete statistical equilibration. Recently collected data taken by the E814 group will be analyzed to look for such an enhancement.

The probability for the cold separation of four neutrons from a projectile is considerably larger if, for example, a more neutron-rich projectile is excited by a heavy target. In fact, the threshold Q value for $^{30}\mathrm{Si}\rightarrow{}^{26}\mathrm{Si}+4n$, -49.6 MeV, is well matched by the excitation energy region covered by second-order excitation. One should bear in mind, however, that second-order excitation may not lead to amplitudes of the collective motion large enough to lead to nonstatistical decay. A signature of the contribution to the total excitation energy by the second-order process would thus be a strong enhancement of the cross sections predicted to first and second order, 19.0 and 1.87 μb respectively, for the $4n$ channel in ^{30}Si.

IV. CONCLUSIONS AND SUMMARY

In this paper we have developed a quantitative framework for the analysis of Coulomb fragmentation processes in collisions or relativistic nuclei. Using the Weizsäcker-Williams method with realistic photoabsorption cross sections, we have shown that multiple GDR excitation processes, although distinct, are always dominated by single-step excitation to the same excitation energy via the quasideuteron process. Beam energies above $\sim$10 GeV/nucleon only lead to enhancement of the first-order cross section, at the expense of a decreased "signal-to-noise" ratio for higher-order excitations. The trend of presently available data is consistent with first-order excitation followed by the statistical decay of the excited nucleus.

Signatures of multiple excitation may be found in ratios of projectile fragmentation cross sections on a light and heavy target. In particular, experimental searches should concentrate on decay channels with threshold Q values near the maximum of the assumed n-fold excitation probability. The present calculations provide a benchmark for what can be expected if statistical effects dominate the decay channels. Strong enhancements of such channels might then provide the first experimental glimpse of the response of nuclei to the absorption of several simultaneous GDR photons.

ACKNOWLEDGMENTS

We would like to thank Johanna Stachel for careful reading of the manuscript. This work was supported in part by the National Science Foundation.

[1]Brookhaven National Laboratory Report 1985.
[2]P. Braun-Munzinger, in *The Response of Nuclei Under Extreme Conditions,* edited by R. A. Broglia and G. F. Bertsch (Plenum, New York, 1988).
[3]C. Brechtmann, W. Heinrich, and E. V. Benton, Phys. Rev. C **39**, 2222 (1989).
[4]C. Brechtmann and W. Heinrich, Z. Phys. A **330**, 407 (1988).
[5]C. Brechtmann and W. Heinrich, Z. Phys. A **331**, 463 (1988).
[6]J. C. Hill, F. K. Wohn, J. A. Winger, and A. R. Smith, Phys. Rev. Lett. **60**, 999 (1988).
[7]M. T. Mercier, J. C. Hill, F. K. Wohn, and A. R. Smith, Phys. Rev. Lett. **52**, 898 (1984).
[8]M. T. Mercier, J. C. Hill, F. K. Wohn, C. M. McCullough, M. E. Nieland, J. A. Winger, C. B. Howard, S. Renwick, D. K. Mathesis, and A. R. Smith, Phys. Rev. C **33**, 1655 (1986).
[9]H. H. Heckman and P. J. Lindstrom, Phys. Rev. Lett. **37**, 56 (1976).
[10]J. Barrette *et al.*, Phys. Rev. C **41**, 1512 (1990).
[11]K. Alder and A. Winther, *Coulomb Excitation* (Academic, New York, 1966).
[12]A. Winther and K. Alder, Nucl. Phys. **A319**, 518 (1979).
[13]E. Fermi, Z. Phys. **29**, 315 (1924).
[14]C. F. Weizsäcker, Z. Phys. **88**, 612 (1934).
[15]E. J. Williams, Phys. Rev. **45**, 729 (1934).
[16]V. M. Budnev, I. F. Ginzburg, G. V. Meledin, and V. G. Serbo, Phys. Rep. C **15**, 183 (1975).
[17]B. Hoffman and G. Baur, Phys. Rev. C **30**, 247 (1984).
[18]G. Baur and C. A. Bertulani, Phys. Rev. C **34**, 1654 (1986).
[19]G. Baur and C. A. Bertulani, Phys. Lett. B **174**, 23 (1986).
[20]G. Baur and C. A. Bertulani, Phys. Rep. C **163**, 299 (1988).
[21]C. A. Bertulani and G. Baur, Nucl. Phys. **A442**, 739 (1985).
[22]J. D. Jackson, *Classical Electrodynamics,* 2nd ed. (Wiley, New York, 1975), Chap. 15.
[23]H. Überall, *Electron Scattering from Complex Nuclei* (Academic, New York, 1971), Vols. A and B.
[24]J. Ahrens, Nucl. Phys. **A446**, 229 (1985).
[25]J. Ahrens *et al.*, Nucl. Phys. **A251**, 479 (1975).
[26]J. Arends, J. Eyink, A. Hegerath, K. G. Hilger, B. Mecking, G. Nöldeke, and H. Rost, Phys. Lett. **98B**, 423 (1981).
[27]A. Bohr and B. Mottelson, *Nuclear Structure* (Benjamin, Reading, 1975), Vol II, Chap. 6.
[28]M. Prakash, P. Braun-Munzinger, J. Stachel, and N. Alamanos, Phys, Rev. C **37**, 1959 (1988).
[29]J. S. Levinger, Phys. Rev. **84**, 43 (1951).
[30]F. Pühlhofer, Nucl. Phys. **A280**, 267 (1977).
[31]E. Kerkove, P. Berkvens, R. Van de Vyver, H. Ferdinande, P. Van Otten, D. Ryckbosch, and E. Van Camp, Nucl. Phys. **A474**, 397 (1984).
[32]D. Ryckbosch, E. Van Camp, R. Van de Vyver, P. Berkvens, E. Kerkove, and P. Van Otten, Nucl. Phys. **A458**, 12 (1986).
[33]K. Snover, Annu. Rev. Nucl. Part. Sci. **36**, 545 (1986).
[34]C. M. Lederer and V. S. Shirley, *Table of Isotopes,* 7th ed. (Wiley, New York, 1978).
[35]W. Dilg, W. Schantl, H. Vonach, and M. Uhl, Nucl. Phys. **A217**, 269 (1973).
[36]A. Gilbert and A. G. W. Cameron, Can. J. Phys. **43**, 1446 (1965).
[37]H. Vonach and M. Hille, Nucl. Phys. **A127**, (1969) 289.